Atomically Smooth *p*-Doped Silicon Nanowires Catalyzed by Aluminum at Low Temperature

Oussama Moutanabbir,[†,*] Stephan Senz,[†] Roland Scholz,[†] Marin Alexe,[†] Yunseok Kim,[†] Eckhard Pippel,[†] Yewu Wang,[†] Christian Wiethoff,[‡] Tobias Nabbefeld,[‡] Frank Meyer zu Heringdorf,[‡] and Michael Horn-von Hoegen[‡]

[†]Max Planck Institute of Microstructure Physics, Weinberg 2, 06120 Halle (Saale), Germany, and [‡]Department of Physics and Center of Nanointegration, Duisburg-Essen (CeNIDE), University of Duisburg-Essen, 47057 Duisburg, Germany

ABSTRACT Silicon nanowires (SiNWs) are powerful nanotechnological building blocks. To date, a variety of metals have been used to synthesize high-density epitaxial SiNWs through metal-catalyzed vapor phase epitaxy. Understanding the impact of the catalyst on the intrinsic properties of SiNWs is critical for precise manipulation of the emerging SiNW-based devices. Here we demonstrate that SiNWs synthesized at low-temperature by ultrahigh vacuum chemical vapor deposition using Al as a catalyst present distinct morphological properties. In particular, these nanowires are atomically smooth in contrast to rough $\{112\}$-type sidewalls characteristic of the intensively investigated Au-catalyzed SiNWs. We show that the stabilizing effect of Al plays the key role in the observed nanowire surface morphology. In fact, unlike Au which induces (111) and (113) facets on the nanowire sidewall surface, Al revokes the reconstruction along the $[\bar{1}\bar{1}2]$ direction leading to equivalent adjacent step edges and flat surfaces. Our finding sets the lower limit of the Al surface density on the nanowire sidewalls at $\sim$2 atom/nm^2. Additionally, despite using temperatures of *ca.* 110−170 K below the eutectic point, we found that the incorporation of Al into the growing nanowires is sufficient to induce an effective *p*-type doping of SiNWs. These results demonstrate that the catalyst plays a crucial role is shaping the structural and electrical properties of SiNWs.

KEYWORDS: silicon nanowire · silicon (112) · metal-catalyzed vapor phase epitaxy · aluminum · surface reconstruction · nanowire doping

The unique properties of silicon nanowires (SiNWs) have inspired a variety of nanoscale technologies. In particular, owing to their strong absorption of sunlight, weak angle dependent and polarization independent response,[1] SiNWs are effective building blocks for photovoltaic cells. In this perspective, several concepts of SiNW-based solar cells have been recently proposed exploiting the morphological and size-related effects as well as the flexibility in the fabrication and design offered by SiNWs and the concomitant progress in probing nanoscale properties.[1−6] Metal-catalyzed vapor-phase epitaxy is a unique synthesis method capable of generating high densities of single crystalline SiNWs.[7] In this process, the growth of SiNWs is accomplished through metal nanoscale clusters, which act catalytically as the energetically favored site for vapor-phase reactant adsorption and when saturated, the nucleation site for crystallization and one-dimensional growth.[7,8] In general, one can distinguish between three categories of catalysts:[9] (1) catalysts with a simple eutectic phase diagram and a eutectic point located at a Si concentration >10 atom %; (2) catalysts with a simple eutectic phase diagram and a eutectic point located at a Si concentration <1 atom %; (3) catalysts with high temperature eutectic points (>800 °C), which also present one or more silicide phases. Au, a type 1 catalyst, is predominantly used for a straightforward and low-temperature synthesis of SiNWs. In this case, tiny AuSi alloy nanoparticles can form by deposition of a thin Au layer on Si and subsequent annealing above the eutectic temperature of the Au−Si system ($\sim$363 °C). The nanowire growth follows either the *classic* three-phase vapor−solid−liquid (VLS) process or the two-phase vapor−solid−solid (VSS) process, which implies the nanowire growth through solid catalyst nanoparticles.[10] In general, for a given metal−semiconductor system, an accurate classification of the growth mode would require, however, the reexamination of the phase diagrams on the nanoscale.[11−13]

The obvious drawback of using Au as a catalyst is the potential deterioration of the optical and electrical properties of SiNWs that can be caused by Au contaminants, which induce deep energy levels in the Si bandgap. These deep levels strongly influence the minority carrier lifetime thereby limiting the efficiency of SiNW-based solar cells as recently suggested.[4] Overcoming this difficulty has sparked a surge of interest

*Address correspondence to moutanab@mpi-halle.mpg.de.

Received for review November 8, 2010 and accepted December 23, 2010.

Published online January 06, 2011
10.1021/nn1030274

© 2011 American Chemical Society

in using non-Au catalysts to grow SiNWs. In this regard, Cu (a type 3 catalyst) was recently presented as an alternative to Au, and Cu-catalyzed SiNWs were demonstrated to perform better (see ref 4 and references therein). This was tentatively attributed to the high diffusivity of Cu in Si and its segregation to the nanowire surface,[4] which can presumably alleviate the nanowire bulk contamination. Nevertheless, the presence of Cu with even trace contamination remains undesired in Si device processing as it generates, for example, a substantial increase in the leakage current of *p-n* junctions,[14] which can be detrimental for solar energy applications. Recently, Al-catalyzed SiNWs (Al–SiNWs) were suggested to be highly suitable to photovoltaic cells.[15,16] For this specific application, the long-standing issue of metal catalyst contamination of the grown SiNWs is no more a concern when Al (a type 1 catalyst) is used. Here, being a shallow acceptor in Si, Al acts as both a catalyst and a dopant yielding *p*-type SiNWs.

In this work, in addition to circumventing the detrimental deep level doping, we demonstrate that the use of Al as a catalyst yields SiNWs with distinct structural and morphological characteristics. In fact, we found that Al–SiNWs display atomically smooth sidewalls in contrast to the rough sidewall surface characteristic to Au-catalyzed SiNWs grown in an ultrahigh vacuum (UHV) environment.[17–21] This absence of sidewalls faceting and irregularities is demonstrated to be due to the stabilizing effect of the SiNW surface by Al atoms. Owing to the high surface-to-volume ratio, the surface structure and morphology define the nanowire transport properties.[22,23] Thus improved charge carrier transport should be expected for smooth nanowires due to the weak surface scattering as compared to rough surfaces. Similarly, the reduced phonon scattering at smooth surfaces can lead to higher thermal conductivity, which is suitable to manage the heat in SiNW-based devices. Smooth surfaces are also convenient for the growth of high quality nanowire heterostructures such as core–shell *p–n* junctions. In addition to the impact of the catalyst atoms on the morphology of the grown nanowires, we also demonstrate that, despite using low growth temperatures (*ca.* 110–170 K below the Al–Si bulk eutectic temperature), the incorporation of Al atoms into the SiNWs during the growth is sufficient to induce an effective *p*-type doping of SiNWs.

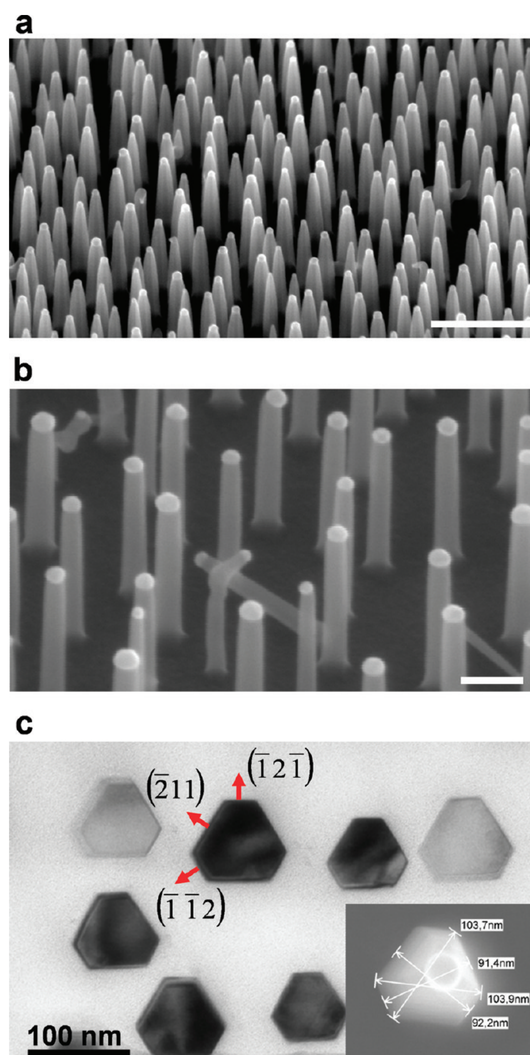

Figure 1. Al–SiNW morphology. (a) SEM image of high-density SiNWs grown at 470 °C. At this temperature, nanowires are slightly tapered and display a narrow size distribution. The scale bar denotes 500 nm. (b) SEM image of straight Al–SiNWs grown at 410 °C. Note that reducing the growth temperature leads to a relatively broader distribution of SiNW size (see Supporting Information, Figure S1). The scale bar denotes 100 nm. (c) Top-view TEM image of radial slices of Al–SiNWs. Inset: Top-view SEM image of individual nanowire.

RESULTS AND DISCUSSION

Al–SiNWs Growth and Morphological Properties. We used an UHV chemical vapor deposition (UHV-CVD) reactor with a background pressure of ~1.0×10^{-10} mbar to grow monocrystalline Al–SiNWs on a Si(111) substrate following the procedure described in ref 24 (see Methods). Unlike the well-established Au-catalyzed growth, the use of Al as a catalyst is very challenging and requires a meticulous control of the experimental parameters and a very clean deposition system because Al is sensitive to impurities and oxidizes rather quickly. Figure 1a shows a scanning electron microscopy (SEM) image of Al–SiNWs grown at the highest temperature (470 °C). A high density ((~$3.81 \pm 0.42) \times 10^9$ cm^{-2}) of uniform nanowires is obtained at a growth rate of ~20 nm/min. The grown nanowires have a height of ~(500 ± 28) nm and a diameter of ~(81 ± 7) nm. The growth at this temperature resulted, however, in slightly tapered nanowires due to the homoepitaxy on the sidewall surfaces, which appears to be significant at this temperature. This tapering is not observed for growth temperatures below 450 °C as demonstrated in Figure 1b displaying a SEM image of straight Al–SiNWs

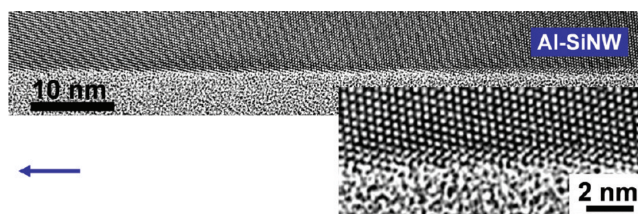

Figure 2. Al–SiNW sidewall surface properties. High resolution XTEM image of SiNW sidewall. Inset is a close-up image of the nanowire surface. Note the absence of short-range as well as long-range surface irregularities and faceting.

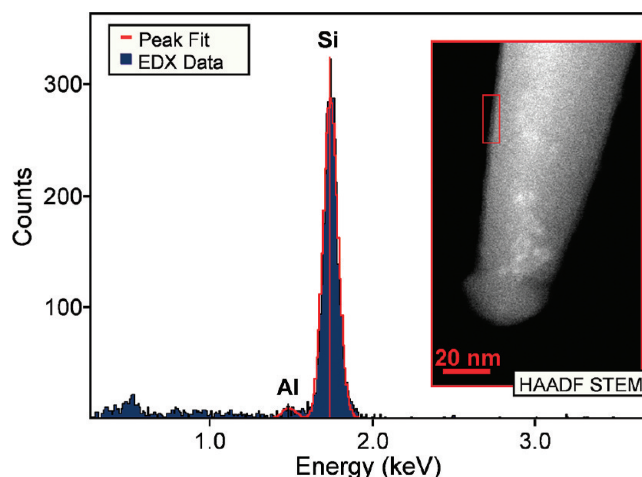

Figure 3. A typical EDX spectrum recorded from the region indicated with the box in the HAADF STEM image shown in the inset. The spectrum displays two peaks in the energy range 1.5–2 keV attributed to Al and Si. The estimated amount of Al in the probed region is about 3 atom %. Note that the observed bright spots in the HAADF image are Cu clusters introduced during the specimen preparation by ion milling (see Supporting Information, Figure S5).

grown at 410 °C. At this temperature, the grown nanowires have a height of ~(241 ± 15) nm and a diameter of ~(37 ± 11) nm. The observed larger diameter at higher temperature is due to higher surface mobility and coarsening of catalyst nanoparticles.[25] We note that the elimination of the nanowire tapering comes, however, with a slight broadening of the nanowire diameter distribution observed at low growth temperature (Supporting Information, Figure S1). Most importantly, in spite of using growth temperatures below the *macroscopic* eutectic temperature of the Al–Si system, one can hardly be conclusive on whether the growth takes place *via* VSS or VLS mode. In fact, earlier observations have shown that the undercooling of Al–Si droplets becomes already significant at a diameter on the order of a few micrometers (Supporting Information, Figure S2).[26] Independently of the growth temperature, the grown nanowires show hexagonal faceting with {211}-type sidewalls (Figure 1c, see also Supporting Information, Figure S3). Identical faceting was previously reported for Au-catalyzed nanowires having a diameter above ~10 nm.[7,17,19–21]

The interesting observation here is that the Al–SiNW sidewall surface is atomically smooth in contrast to Au-catalyzed SiNWs, which display a faceted and rough sidewalls surface. This can be clearly seen in Figure 2 showing a high resolution transmission electron microscopy (TEM) image of Al–SiNW (see also Supporting Information, Figure S4). *In situ* electron microscopy studies have demonstrated that the roughness of Au-SiNWs originates from a periodic sawtooth faceting[17] resulting from Au-induced (111) and (113) facets on the Si(112) sidewall surface.[18] Analogously, it is plausible that the nature of the interaction of Al atoms with the Si(112) surface may play the key role in defining the morphology of the Al–SiNW sidewalls since the presence of Al catalyst atoms on the nanowire surface is inevitable as it seems to be energetically favorable as suggested by recent calculations.[27] Nevertheless, no evidence of Al in the investigated nanowires can be obtained from our high resolution TEM/STEM images. This is because Al and Si have very close atomic numbers which makes them undistinguishable in TEM imaging unlike Au which presents a clear contrast in Si making straightforward its detection in Au-SiNWs.[28] However, our systematic elemental analysis shows that the regions near the sidewalls of the grown nanowires contain Al in a sufficient amount to be detectable by energy-dispersive X-ray spectroscopy (EDX). Figure 3 displays a representative EDX spectrum recorded from the region near the sidewall of Al–SiNW indicated by the box in the high angle annular dark field (HAADF) STEM image (inset). The probed region extends from the surface of the nanowire to a depth of *ca.* 1–4 nm below the surface. The spectrum displays two peaks in the energy

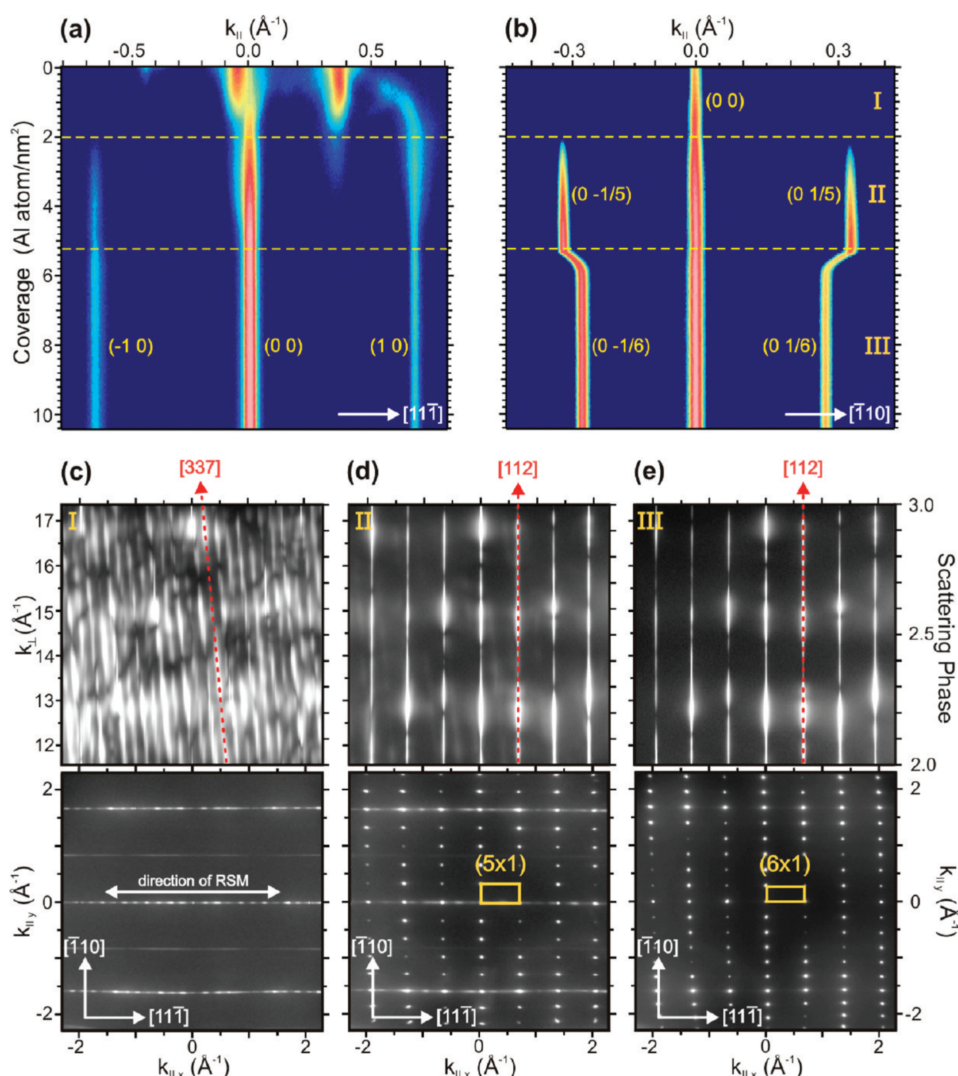

Figure 4. Al influence on Si(112) surface structure and morphology: (a) *in situ* 1D-SPA-LEED spot profiles in [11$\bar{1}$] direction as a function of Al coverage on S(112); (b) *in situ* SPA-LEED spot profiles in [$\bar{1}$10] direction as a function of Al coverage on S(112); (c) RSM along [11$\bar{1}$] direction and the 2 × 1 diffraction pattern at an Al coverage of 0.6 atom/nm^2 in phase A; (111) and (337) facets are observed, which is characteristic of undisturbed Si(112); (d) RSM along [11$\bar{1}$] direction and diffraction pattern at an Al coverage of 4.3 atom/nm^2 in phase B. Only (112) rods are observed. The diffraction pattern indicates 5-fold periodicity. (e) RSM along [11$\bar{1}$] direction and diffraction pattern at an Al coverage of 7.8 atom/nm^2 in phase C. Only (112) rods are observed. The diffraction pattern indicates 6-fold periodicity.

range 1.5−2 keV associated with Al and Si. Note that the observed bright spots in the image (inset) correspond to Cu contaminants introduced during the preparation of TEM specimens (Supporting Information, Figure S5).

The Role of Al Atoms in Shaping the Nanowire Surface. As mentioned above, the observed morphology of Al−SiNWs (Figure 2) may result from the interaction of Al atoms with the {112}-type sidewalls of the growing nanowires. To test this hypothesis, we investigated the behavior of Al atoms on Si(112) surface. In general, the Si(112) surface is composed of quasiperiodic nanoscale facets. Each nanofacet consists of a single unit cell wide (111) terrace opposed by a 6 to 11 nm (337) terrace.[29] This unique faceting results from the low free energy of a single unit cell of the Si(111) (7 × 7) reconstruction combined with the stability of reconstructed Si(337). Substantial rearrangements in Si(112) nanofaceting were observed upon exposure to a fraction of monolayer of various metals.[30−33] In the following, we elucidate the interaction of Al atoms with the Si(112) surface and its implication for the morphology of the Al−SiNW sidewall surface. Toward this end, we used spot-profile-analyzing low-energy electron diffraction (SPA-LEED)[34,35] to probe *in situ* the faint changes in the structural characteristics of clean Si(112) surface exposed to Al atoms (see Methods). To obtain the Al-induced structural and morphological changes in the Si(112) surface, one-dimensional (1D) SPA-LEED scans were recorded at different Al surface densities using a RHEED-like geometry.[36] Moreover, to establish the role of Al in tailoring nanofacet orientations, we used SPA-LEED to record the evolution of reciprocal space maps (RSMs), which represent the surface lattice

rods in the reciprocal space. These RSMs are a precise measure of the structural and morphological properties of the investigated surface.

Figure 4 panels a and b show *in situ* 1D-SPA-LEED spot profiles recorded for an increasing amount of Al on Si(112) surface along the two perpendicular directions [11$\bar{1}$] and [$\bar{1}$10], respectively. The two sets of profiles were measured simultaneously. We note that two spots are observed along [11$\bar{1}$] for the initial surface (Figure 4a). These spots are diffuse as expected from the surface disorder in this direction.[29] At Al coverage of ~1 atom/nm^2, these spots vanish and new, relatively sharp spots appear at 0 and −0.67 Å^{-1}. A third spot at +0.67 Å^{-1} emerges later at Al coverage of ~3 atom/nm^2. Each of the observed spots is associated with a distinct surface morphology with characteristic stepped surfaces and nanofacets. As shown below, the observed new spots are the (−1 0) and the (1 0) of the (112) surface, corresponding to unit cell size of 9.41 Å. The increase of Al coverage up to ~4.4 atom/nm^2 enhances the sharpness of the spots, which can be understood as an increase in the surface order along the [11$\bar{1}$] direction. Additional deposition of Al beyond this coverage does not induce any change in the 1D-SPA-LEED profiles, indicating that the surface has reached a steady-state. Interestingly, the profiles along the [$\bar{1}$10] direction (corresponding to the ordered direction[29]) show three clear phases. Below ~2 atom/nm^2 (phase I), one spot is observed at 0 Å^{-1} and appears to be insensitive to Al. Above ~2 atom/nm^2 (phase II) two spots (0 −1/5) and (0 1/5) emerge around ±0.33 Å^{-1}. Beyond ~5.2 atom/nm^2, these spots smoothly shift inward to smaller momentum transfer of ±0.27 Å^{-1} corresponding to (0 −1/6) and (0 1/6) spots (phase III). Note that the obtained 1D-SPA-LEED profiles are independent of the substrate temperature and do not change even if the temperature increases above 470 °C (up to 700 °C).

To gain more insights into the detailed step structure, RSMs were obtained for each coverage-dependent phase. Figure 4c shows the RSM and LEED diffraction pattern for phase I. The dominant features are (337) reciprocal lattice rods which, under closer inspection, exhibit a fine structure which is caused by an ordered step sequence with a terrace width of 115 ± 15 Å and a step height of 8.0 ± 0.5 Å. We conclude that for phase I (less than *ca.* 2 Al/nm^2) Al atoms stabilize regularly stepped (337) facets. The relatively large step height of 8 Å is explained by the formation of ultranarrow (111) facets of a width of only half of the (7 × 7) unit cell as already observed for the clean Si(112) surface.[29] Such a step height of 7.96 Å is in agreement with our measurement. Because these (111) facets exhibit a width of only 23 Å they do not show up in the LEED pattern. A significant change is, however, detected in the RSM of the phase II (Figure 4d). Remarkably, only the (112) reciprocal lattice rods are observed. Note that the (112) rods do not exist in a pristine (112) surface. Furthermore, a 5-fold periodicity is established in phase II. For the phase III, the same (112) reciprocal lattice rods are detected with 6-fold reconstructions parallel to the step edges (Figure 4e). This drives us to conclude that the observed 1D-SPA-LEED spots (0 ± 1/5) and (0 ± 1/6) in phases II and III correspond to atomically flat Si(112) (5 × 1) and Si(112) (6 × 1) surfaces, respectively.

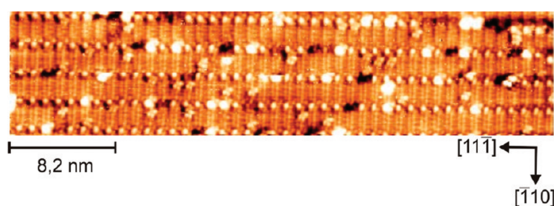

Figure 5. Al-stabilized Si(112) surface. Scanning tunneling microscopy image of the Al−Si(112) (6 × 1) surface (phase III). The image obtained with 0.6 nA tunnel current at a bias voltage of −2.1 V displays filled states. Ordered atomic chains of Al are visible along the step edges.

The results described above demonstrate that the presence of Al atoms on the Si(112) surface revokes the reconstruction along the [$\bar{1}\bar{1}$2] direction leading to equivalent adjacent step edges. Based on earlier observations,[37] models of the corresponding Al-induced (5 × 1) and (6 × 1) surface reconstructions are presented in Supporting Information, Figures S6 and S7. Moreover, the observed 6-fold periodicity was found to originate from the formation of Al atomic chains along the step edges evidenced by *in situ* scanning tunneling microscopy investigations of the Si(112) surface performed at phase III as shown in Figure 5. It is clear that Al strongly stabilizes the Si(112) surface unlike Au, which induces a multitude of coverage-dependent facets and exhibits (111) and (113) nanofacets on Si(112) responsible of the rough sawtooth-like sidewalls of Au-catalyzed SiNWs.[17−21] The absence of clear stepped surfaces in high resolution XTEM images (Figure 2) agrees with the SPA-LEED data demonstrating that the stabilizing effect of Al atoms is behind the grown atomically smooth nanowires. These observations set the lower limit of the Al surface density on the nanowire sidewalls at ~2 atom/nm^2.

***p*-type Doping through the Incorporation of Al Catalyst Atoms.** Besides the aforementioned influence of Al on the structural and morphological properties of Al−SiNW surface, the incorporation of Al into the growing nanowires is expected to yield *p*-type doping. Indeed, calculations of the formation energy of Al-related defects in SiNW suggest that the formation of Al substitution impurities in SiNW is favored over the occupation of interstitial sites.[27] Al is a single acceptor, thus its incorporation during the growth leads to *p*-type SiNWs as was recently observed .[15,16] To investigate the possible incorporation of Al into SiNWs grown

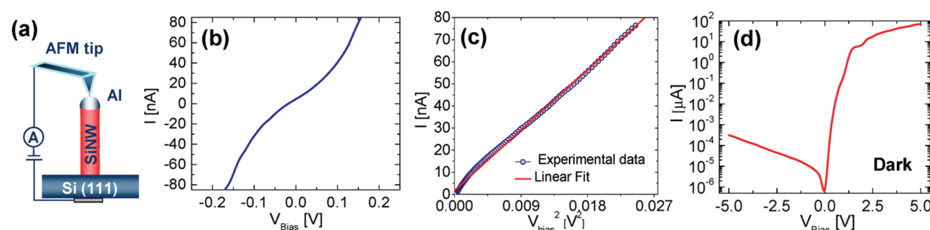

Figure 6. Electrical properties of Al−SiNWs. (a) Schematic illustration of C-AFM measurement of the electrical properties a single nanowire. (b) The *I*−*V* characteristic curve of a single Al−SiNW grown on a *p*-type Si(111). (c) *I*−V^2 characteristic curve of a single Al−SiNW grown on a *p*-type Si(111) (circles). The sold line corresponds to the best linear fit of the experimental data. (d) The *I*−*V* characteristic curve of a single Al−SiNW grown on a *n*-type Si(111). Note that the *I*−*V* curves recorded immediately after a dip in a diluted HF solution were found to be identical to those recorded for as-grown nanowires.

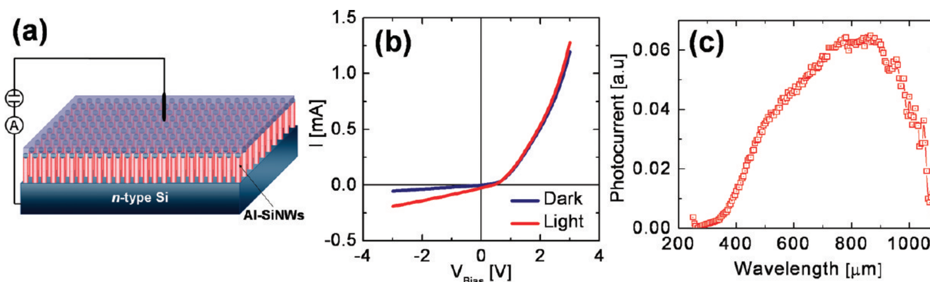

Figure 7. (a) Schematic illustration of a device made of an array of Al−SiNWs vertically aligned on *n*-type Si(111). For the fabrication of the device, as-grown Al−SiNWs were first capped in a polymer. By using reactive ion-etching, the deposited polymer cap was partially etched until the tips of the SiNWs emerge. Afterward, a metal contact was deposited by evaporation on an area containing up to ∼9 × 10^4 nanowires. (b) The dark and under illumination *I*−*V* characteristic curves of the device described in panel a. Note that the reverse current does not reach the saturation and instead increases linearly as a function of the applied voltage. This phenomenon is attributed to surface leakage,[39] which becomes important due to the high surface-to-volume ratio associated with the geometry of the nanowire. (c) The spectral distribution of the generated photocurrent in the device described in panel a.

at 410 °C, the current−voltage characteristics (*I*−*V* curves) of individual Al−SiNWs still attached to the substrate were measured using conductive atomic force microscopy (C-AFM) as illustrated in Figure 6a. Two sets of samples were probed using this setup. The first set consists of single Al−SiNW grown on a *p*-type Si(111) at 410 °C. Figure 6b shows the *I*−*V* curve of a single nanowire measured in the range of −0.2 to 0.2 V. The observed deviation of the *I*−*V* curve from the linear behavior originates from space-charge-limited current.[38] Indeed, a quadratic *I*−*V* characteristic ($I \propto V^2$) is obtained for Al−SiNWs grown on *p*-type Si(111) as shown in Figure 6c. Interestingly, the *I*−*V* curve of the second set of Al−SiNWs grown on a *n*-type Si(111) is similar to the characteristic curve of a *p*−*n* junction (Figure 6d). This provides clear evidence that the grown SiNWs are *p*-doped as a result of the incorporation of Al atoms during the growth at a temperature as low as 410 °C. Nevertheless, at this stage, the doping level in the as-grown Al−SiNWs can hardly be quantified with confidence. However, the fact that these nanowires are very uniform with high-density (Figure 1) can be exploited to implement a device made of an array of vertically aligned as-grown Al−SiNWs grown on *n*-type Si(111) as schematically illustrated in Figure 7a. The device was fabricated by capping the as-grown Al−SiNWs with a polymer layer. Using reactive ion-etching, the deposited polymer cap was partially etched until the tips of the SiNWs emerge. Afterward, a metal contact was deposited by evaporation on an area containing up to ∼9 × 10^4 nanowires. We found that this device behaves as a well-defined *p*−*n* junction (Figure 7b). The spectral distribution of the photocurrent generated by this array of as-grown Al−SiNWs is identical to a Si-based photodiode (Figure 7c). It emerges from these observations that, despite the relatively low growth temperature, the incorporation of Al is sufficient to induce an effective *p*-type doping in as-grown Al−SiNWs. This makes Al−SiNWs of some relevance to photovoltaic applications.

CONCLUSION

Our work demonstrates that the catalyst atoms play a critical role in shaping the structural and electrical properties of SiNWs synthesized by metal-catalyzed vapor phase epitaxy in an UHV-CVD reactor. We have found that the use of Al as a catalyst leads to atomically smooth SiNWs in contrast to the rough {112}-type sidewalls observed in Au-catalyzed SiNWs. This effect is attributed to the Al stabilizing effect of Si(112) surfaces, which manifests by revoking the reconstruction along the $[\bar{1}\bar{1}2]$ direction leading to equivalent adjacent step edges and flat surfaces. This finding suggests that the Al density on the nanowire surface is at least 2 atom/nm^2. Smooth nanowire surfaces present certain

advantages expected from the weak charge carrier and phonon scattering. Smooth surfaces are also convenient for radial overgrowth used in the fabrication of nanowire core−shell heterostructures. Nevertheless, the Al high surface density might cause some difficulties in controlling the overgrowth on Al−SiNWs. This issue can be overcome through *ex situ* cleaning of the as-grown nanowires using treatments (*e.g.*, HNO_3:HCl solutions) that can selectively etch Al. Additionally, we found that the growth at low temperatures (up to 170 K below the Al−Si bulk eutectic temperature) is associated with a significant incorporation of Al atoms into the growing nanowires leading to an effective *p*-type doping of SiNWs.

METHODS

Nanowire Growth. Phosphorus- and boron-doped Si(111) wafers were used as substrates in our experiments. The substrates surface was conditioned by a standard wet chemical cleaning followed by a dip in 2% hydrofluorid acid to hydrogen-passivate the surface. The wafers were immediately transferred into the UHV-CVD reactor. A 1 nm-thick Al film was then deposited *in situ* on the substrate by a thermal evaporation source. Immediately after Al deposition, the substrate was annealed for 30 min at 600 °C. The growth of Al−SiNWs was accomplished by using monosilane (diluted to 5% in argon) as a precursor in the temperature range of ∼400−470 °C, which is below the Al−Si bulk eutectic point (577 °C). The partial pressure of the silane was kept below 0.15 mbar during the growth.

Morphology: Electron Microscopy. The morphology of Al−SiNWs was characterized using a FEI Dualbeam Nanolab 600 scanning electron microscope, a Philips CM 20T transmission electron microscope operating at 200 kV, JEOL JEM-4010 transmission electron microscope operating at 400 kV, and aberration-corrected (Cs probe corrector) FEI TITAN 80−300 analytical scanning transmission electron microscope operating at 300 kV and allowing a spatial resolution of about 100 pm in both modes. In addition, this microscope is also equipped with an energy dispersive X-ray (EDX) detector having a detection limit of about 0.5 at.%.

Surface Properties: 1D-SPA-LEED. Spot profile analyzing low energy electron diffraction (SPA-LEED) was performed in a UHV system with a background pressure of 2×10^{-10} mbar. Spot profiles were measured *in situ* during adsorption using a second electron gun in a RHEED-like geometry at an incident angle of 57.4°. After quenching to room temperature reciprocal space maps were obtained under normal incidence using the internal electron gun of the SPA-LEED. Si(112) samples with an azimutal miscut of less than 0.2° were used in this study. The samples were degassed at 600 °C for at least 24 h in high vacuum at a background pressure of 10^{-7} mbar. Al was deposited using a filament heated graphite crucible at rates of 0.07−0.11 monolayer/min (1 monolayer on a Si(111) surface $\sim 7.8 \times 10^{14}$ atoms/cm^2). The evaporated mass flux was calibrated using the Al ($3^{1/2} \times 3^{1/2}$) reconstruction on Si(111), which corresponds to $^1/_3$ of a monolayer. To obtain the Al-induced structural and morphological changes in the Si(112) surface, one-dimensional (1D) SPA-LEED scans were recorded at different Al surface densities using a RHEED-like geometry.[36] We used an electron energy of 122.6 eV at a grazing angle of 32.6° corresponding to a vertical momentum transfer of 6.11 $Å^{-1}$ or an electron scattering phase of S = 1.08 for the {112} step height of 1.11 Å.

Electrical Properties: Conductive Atomic Force Microscopy. The local electrical measurements were performed using a conductive atomic force microscopy (C-AFM) module of a commercial AFM (XE-100, Park Systems). The measured current was calibrated using a 100 kOhm resistor. The local current−voltage (*I*−*V*) characteristics of Si nanowires were carried out by C-AFM under applying voltages to the bottom electrode. Au/Cr-coated silicon cantilevers (NSC18/Au−Cr, MikroMasch) with a spring constant of 3.5 N/m and a resonant frequency of 75 kHz were used as a movable top electrode to apply voltage bias.

Supporting Information Available: Detailed analysis of Al−SiNWs morphology, comparison of the sidewall structures in Au-SiNW *vs* Al−SiNW, influence of undercooling on the Al−Si phase diagram, and models of Al-induced (5 × 1) and (6 × 1) reconstruction of the Si(112) surface. This material is available free of charge *via* the Internet at http://pubs.acs.org.

Note Added After Asap Publication: Due to a production error this paper was published without its funding acknowledgments. The corrected version was published on January 10, 2011.

Acknowledgment. This paper has been dedicated to the memory of Ulrich Gösele. O.M. acknowledges funding from the German Ministry of Education and Research (BMBF) under contracts No. 01BU0624 (CRYSGAN) and No. 13 N 9881 (DECISIF). The authors are grateful to Ursel Doß, Kai-Uwe Aßmann, and Horst Blumtritt for their technical assistance.

REFERENCES AND NOTES

1. Ciao, L.; Fan, P.; Vasudev, A. P.; White, J. S.; Yu, Z.; Cai, W.; Schuller, J. A.; Fan, S.; Brongersma, M. L. Semiconductor Nanowire Optical Antenna Solar Absorbers. *Nano Lett.* **2010,** *10*, 439–445.
2. Tian, B.; Kempa, T. J; Lieber, C. M. Single Nanowire Photovoltaics. *Chem. Soc. Rev.* **2009,** *38*, 16–24.
3. Garnett, E.; Yang, P. Light Trapping in Silicon Nanowire Solar Cells. *Nano Lett.* **2010,** *10*, 1082–1087.
4. Boettcher, S. W.; Spurgeon, J. M.; Putnam, M. C.; Warren, E. L.; Turner-Evans, D. B.; Kalzenberg, M. D.; Miolo, J. R.; Atwater, H. A.; Lewis, N. S. Energy-Conversion Properties of Vapor−Liquid−Solid Grown Silicon Wire-Array Photocathodes. *Science* **2010,** *327*, 185–187.
5. Kelzenberg, M. D.; Boettcher, S. W.; Petykiewicz, J. A.; Turner-Evans, D. B.; Putnam, M. C.; Warren, E. L.; Spurgeon, J. M.; Briggs, R. M.; Lewis, N. S.; Atwater, H. A. Enhanced Absorption and Carrier Collection in Si Wire Arrays for Photovoltaic Applications. *Nat. Mater.* **2010,** *9*, 239–244.
6. Garnett, E. C.; Yang, P. Silicon Nanowire Radial *p*−*n* Junction Solar Cells. *J. Am. Chem. Soc.* **2008,** *130*, 9224–9225.
7. Wagner, R. S.; Ellis, W. C. Vapor−Liquid−Solid Mechanism of Single Crystal Growth. *Appl. Phys. Lett.* **1964,** *4*, 89–90.
8. Schwarz, K. W.; Tersoff, J. From Droplets to Nanowires: Dynamics of Vapor−Liquid−Solid Growth. *Phys. Rev. Lett.* **2009,** *102*, 206101 1–4.
9. Schmidt, V.; Wittemann, J. V.; Senz, S.; Gösele, U. Silicon Nanowires: A Review on Aspects of their Growth and their Electrical Properties. *Adv. Mater.* **2009,** *21*, 2681–2702.
10. Kodambaka, S.; Tersoff, J.; Reuter, M. C.; Ross, F. M. Germanium Nanowire Growth below the Eutectic Temperature. *Science* **2007,** *316*, 729–732.
11. Kim, B. J.; Tersoff, J.; Wen, C.-Y.; Reuter, M. C.; Stach, E. A.; Ross, F. M. Determination of Size Effects during the Phase Transition of a Nanoscale Au−Si Eutectic. *Phys. Rev. Lett.* **2009,** *103*, 155701 1–4.
12. Sutter, E.; Sutter, P. Phase Diagram of Nanoscale Alloy Particles Used for Vapor−Liquid−Solid Growth of Semiconductor Nanowires. *Nano Lett.* **2008,** *8*, 411–414.
13. Schwalbach, E. J; Voorhees, P. W. Phase Equilibrium and Nucleation in VLS-Grown Nanowires. *Nano Lett.* **2008,** *8*, 3739–3745.
14. Istratov, A. A.; Weber, E. R. Physics of Copper in Silicon. *J. Electrochem. Soc.* **2002,** *149*, G21–G30.
15. Wacaser, B. A.; Reuter, M. C.; Khayyat, M. M.; Wen, C.-Y.; Haight, R.; Guha, S.; Ross, F. M. Growth System, Structure,

and Doping of Aluminum-Seeded Epitaxial Silicon Nanowires. *Nano Lett.* **2009,** *9*, 3296–3301.
16. Ke, Y.; Weng, X.; Redwing, J. M.; Eichfeld, C. M.; Swisher, T. R.; Mohney, S. E.; Habib, Y. M. Fabrication and Electrical Properties of Si Nanowires Synthesized by Al Catalyzed Vapor−Liquid−Solid Growth. *Nano Lett.* **2009,** *9*, 4494–4499.
17. Ross, F. M.; Tersoff, J.; Reuter, C. M. Sawtooth Faceting Silicon Nanowires. *Phys. Rev. Lett.* **2005,** *95*, 146104 1–4.
18. Wiethoff, C.; Ross, F. M.; Copel, M.; Horn-von Hoegen, M.; Meyer zu Heringdorf, F.-J. Au Stabilization and Coverage of Sawtooth Facets on Si Nanowires Grown by Vapor−Liquid−Solid Epitaxy. *Nano Lett.* **2008,** *8*, 3065–3068.
19. Li, F.; Nellist, P. D.; Cockayne, D. J. H. Doping-Dependent Nanofaceting on Silicon Nanowire Surfaces. *Appl. Phys. Lett.* **2009,** *94*, 263111 1–3.
20. Xu, T.; Nys, J. P.; Addad, A.; Lebedev, O. I.; Urbieta, A.; Salhi, B.; Berthe, M.; Grandidier, B.; Stiévenrad, D. Faceted Sidewalls of Silicon Nanowires: Au-Induced Structural Reconstructions and Electronic Properties. *Phys. Rev. B* **2010,** *81*, 115403 1–10.
21. Li, F.; Nellist, P. D.; Lang, C.; Cockayne, D. J. H. Dependence of Surface Facet Period on the Diameter of Nanowires. *ACS Nano* **2010,** *4*, 632–636.
22. Jie, J.; Zhang, W.; Peng, K.; Yuan, G.; Lee, C. S.; Lee, S.-T. Surface-Dominated Transport Properties of Silicon Nanowires. *Adv. Funct. Mater.* **2008,** *18*, 3251–3257.
23. Martin, P.; Aksamija, Z.; Pop, E.; Ravaioli, U. Impact of Phonon-Surface Roughness Scattering on Thermal Conductivity of Thin Si Nanowires. *Phys. Rev. Lett.* **2009,** *102*, 125503 1–4.
24. Wang, Y.; Schmidt, V.; Senz, S.; Gösele, U. Epitaxial Growth of Silicon Nanowires Using Aluminium Catalyst. *Nat. Nanotechnol.* **2006,** *1*, 186–189.
25. Hannon, J. B.; Kodambaka, S.; Ross, F. M.; Tromp, R. M. The Influence of the Surface Migration of Gold on the Growth of Silicon Nanowires. *Nature* **2006,** *440*, 69–71.
26. Das, S. K.; Perepezko, J. H.; Wu, R. I.; Wilde, G. Undercooling and Glass Formation in Al-Based Alloys. *Mater. Sci. Eng., A* **2001,** *304*−*306*, 159–165.
27. Rurali, R.; Cartoixa, X. Theory of Defects in One-Dimensional Systems: Application to Al-Catalyzed Si Nanowires. *Nano Lett.* **2009,** *9*, 975–979.
28. Allen, J. E.; Hemesath, E. R.; Perea, D. E.; Lensch-Falk, J. L.; Li, Z. Y.; Yin, F.; Gass, M. H.; Wang, P.; Bleloch, A. L.; Palmer, R. E.;; *et al* High-Resolution Detection of Au Catalyst Atoms in Si Nanowires. *Nat. Nanotechnol.* **2008,** *3*, 168–173.
29. Baski, A. A.; Whitman, L. J. Quasiperiodic Nanoscale Faceting of High-Index Si Surface. *Phys. Rev. Lett.* **1995,** *74*, 956–959.
30. Baski, A. A.; Whitman, L. J. Ga-Induced Restructuring of Si(112) and Si(337). *J. Vac. Sci. Technol. B* **1996,** *14*, 992–994.
31. Gai, Z.; Zhao, R. G.; Yang, W. S.; Sakurai, T. Atomic Structure of the Si(112) 7 × 1-In Surface. *Phys. Rev. B* **2000,** *61*, 9928–9931.
32. Zavitz, D. H.; Evstigneeva, A.; Singh, R.; Fulk, C.; Trenary, M. Influence of Arsenic on the Atomic Structure of the Si(112) Surface. *J. Electron. Mater.* **2005,** *34*, 839–845.
33. Cho, E. S.; Kim, M. K.; Park, J. W.; Hur, H.; Jeon, C.; Baik, J. Y.; Hwang, C. C.; Kang, T. H.; Kim, B.; An, K. S.; *et al.* Photoemission Study on the Sb-Induced Reconstruction of the Si(112) Surfaces. *Surf. Sci.* **2005,** *591*, 38–44.
34. Scheithauer, U.; Meyer, G.; Henzler, M. A New LEED Instrument for Quantitative Spot Profile Analysis. *Surf. Sci.* **1986,** *178*, 441–451.
35. Horn-von Hoegen, M. Growth of Semiconductor Layers Studied by Spot Profile Analysing Low Energy Electron Diffraction—Part I. *Z. Kistallogr.* **1999,** *214*, 591–629.
36. Meyer zu Heringdorf, F.-J.; Horn-von Hoegen, M. Reciprocal Space Mapping by Spot Profile Analyzing Low Energy Electron Diffraction. *Rev. Sci. Instrum.* **2005,** *76*, 085102 1–5.
37. Jung, T. M.; Prokes, S. M.; Kaplan, R. Growth and Energetics of Ga and Al Chains on Si(112). *J. Vac. Sci. Technol. A* **1994,** *12*, 1838–1842.
38. Alec Talin, A.; Leonard, F.; Swartzentruber, B. S.; Wang, X.; Hersee, S. D. Unusually Strong Space-Charge-Limited Current in Thin Wires. *Phys. Rev. Lett.* **2008,** *101*, 076802 1–4.
39. Cutler, M; Bath, M. H. Surface Leakage Current in Rectifiers. *J. Appl. Phys.* **1954,** *25*, 1440–1441.